Controlling dual Mott states by hydrogen doping to perovskite rare-earth nickelates

Ikuya Matsuzawa,[1] Takahiro Ozawa,[1,*] Yusuke Nishiya,[1] Umar Sidik,[2] Azusa N. Hattori,[2] Hidekazu Tanaka,[2] and Katsuyuki Fukutani[1,3,†]

[1]*Institute of Industrial Science, The University of Tokyo, Komaba Meguro-ku, Tokyo 153-8505, Japan*
[2]*SANKEN, Osaka University, Ibaraki, Osaka 567-0047, Japan*
[3]*Advanced Science Research Center, Japan Atomic Energy Agency (JAEA), Tokai, Ibaraki 319-1195, Japan*

(Received 1 May 2023; revised 26 June 2023; accepted 8 August 2023; published 24 August 2023)

Doping hydrogen in correlated oxides is a promising way to control the materials functionalities. With *in situ* measurements of the resistance and hydrogen concentration by a nuclear reaction analysis, we have derived the detailed relation between the resistance and hydrogen concentration (x) for $R\mathrm{NiO_3H}_x$ (R = Sm, Nd, and La), which reveal a clear resistance jump at a certain concentration. Taking account of the spatial distribution of hydrogen in both in-plane and depth directions, we have clarified that an insulating state is realized at $x = 0.5$ and another insulating state is formed at $x = 1$. The electronic mechanisms for the two states are proposed in terms of Mott phases.

DOI: 10.1103/PhysRevMaterials.7.085003

I. INTRODUCTION

Strongly correlated oxides reveal fascinating functionalities including electric, magnetic, and optical properties, which can be controlled by external stimuli. The rare-earth nickelates ($R\mathrm{NiO_3}$, R = rare-earth element) with a perovskite structure reveal a thermally induced metal-to-insulator transition (MIT), which has been a topic of intensive studies to date [1–3]. Whereas the electronic state of $R\mathrm{NiO_3}$ is understood in terms of the negative charge transfer between Ni cations and O anions [4,5], various physical mechanisms for this MIT have been discussed including orbital, charge, and spin ordering [3]. The structural analysis shows the presence of two inequivalent Ni sites indicating disproportion of the Ni-O bond length. Based on this result, a novel charge order state has recently been proposed for the insulating state [6–8].

Recently, it was reported that hydrogen doping to $R\mathrm{NiO_3}$ as an external stimulus induces a colossal MIT [9,10], which finds numerous applications such as sensors [11], energy conversion devices [12], and reconfigurable electronics [13]. Since hydrogen often acts as an electron donor, it has been tacitly believed that electron doping changes the nominal valence state of Ni^{3+} with the $3d^7$ ($t_{2g}^6 e_g^1$) configuration [Fig. 1(a)] to Ni^{2+} $3d^8$ ($t_{2g}^6 e_g^2$) resulting in a Mott insulating state as schematically shown in Fig. 1(c). Although a reduction of Ni from Ni^{3+} to Ni^{2+} by H doping was confirmed by x-ray photoelectron spectroscopy (XPS) and x-ray absorption fine structure, the H doping level in $R\mathrm{NiO_3}$ is controversial. In recent studies [14,15], the hydrogen concentration doped in $\mathrm{SmNiO_3}$ was quantified to be less than a few at. % by a nuclear reaction analysis (NRA) [16,17], which was much lower than expected, and an alternative mechanism is discussed in relation to the lattice distortion and transient H diffusion [14,15]. Since NRA measurements were performed *ex situ* in these studies, however, the hydrogenated sample could be dehydrogenated by exposure to air [9]. Therefore, the relation between the hydrogen doping level and electronic phase of $R\mathrm{NiO_3}$ remains to be elucidated. As well as $R\mathrm{NiO_3}$, the electronic phase was substantially modified by hydrogen doping for other correlated oxides such as VO_2 [18], $SrCoO_{2.5}$ [19], and Sr_2IrO_4 [20]. In these regards, clarifying the relation between the electronic phase and hydrogen concentration is strongly required for understanding the mechanism of H-induced phase modulation.

In the present paper, we have developed an apparatus that allows us to *in situ* measure the resistance and hydrogen concentration in the sample with NRA as schematically shown in Fig. 1(e). With this apparatus, we derived a detailed relation between the resistance and hydrogen concentration (x) for $R\mathrm{NiO_3H}_x$ (R = Sm, Nd, and La). With an aid of optical-image observation, hydrogenation was found to be inhomogeneous for R = Nd and La, while the entire film of $\mathrm{SmNiO_3}$ was uniformly hydrogenated. Based on these results, we show an insulating state is realized at $x \sim 0.5$ and another insulating phase is formed at $x = 1$. We propose an electronic mechanism for H-induced MIT, which corresponds to Mott insulators.

II. EXPERIMENTAL METHOD

The samples investigated in the present study are thin films of $R\mathrm{NiO_3}$ (R = Sm, Nd, and La) with a size of 8×8 mm^2 and a thickness of about 80 nm fabricated by pulsed-laser deposition [21]. Films of R = Sm and La were grown on $\mathrm{LaAlO_3}(001)$ and $\mathrm{SrTiO_3}(001)$, respectively, and films of R = Nd were fabricated on both $\mathrm{LaAlO_3}(001)$ and $\mathrm{SrTiO_3}(001)$. Epitaxial growth of the films in the (001) direction was confirmed by x-ray diffraction. To induce dissociation of hydrogen molecules and subsequent hydrogenation of the samples, a mesh-patterned Pt layer (10×10 μm^2) with a

*t-ozawa@iis.u-tokyo.ac.jp
†fukutani@iis.u-tokyo.ac.jp

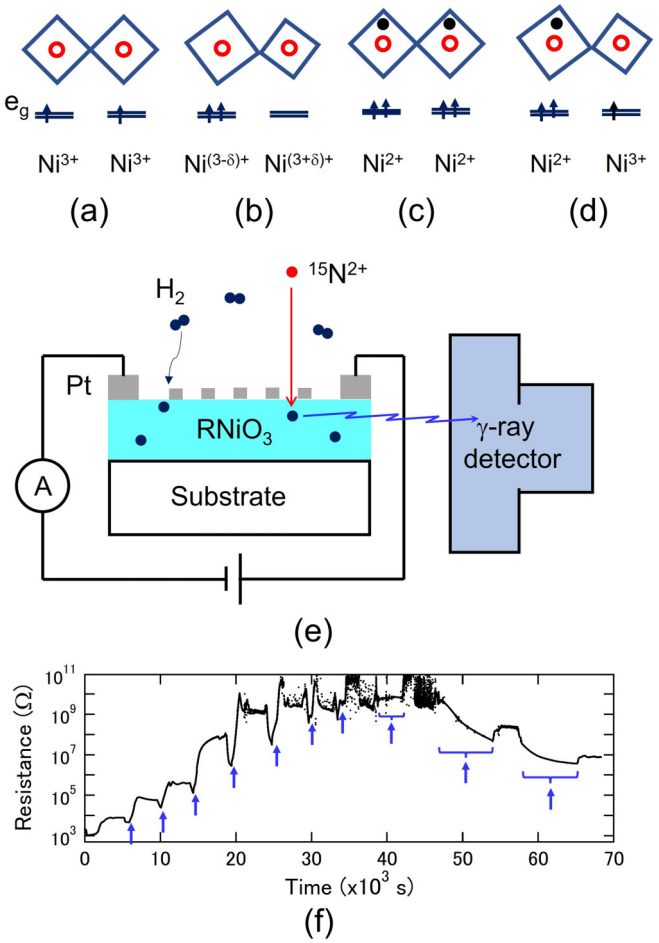

FIG. 1. (a)–(d) Schematic NiO_6 structures and the energy levels of the Ni e_g orbital. Red open circles and black solid circles denote Ni and H ions, respectively, and squares represent oxygen octahedra. Pristine $R NiO_3$ in the (a) metallic state, (b) insulating state, (c) hydrogenated $R NiO_3$ at $x = 1$, and (d) hydrogenated $R NiO_3$ at $x = 0.5$. (e) Schematic experimental setup for *in situ* NRA and resistance measurements. $^{15}N^{2+}$ ions are incident to the samples in the normal direction, and NRA events are detected by γ-ray detectors. Because Pt islands are deposited on the sample as hydrogenation catalysts, part of $^{15}N^{2+}$ ions suffer from an energy loss by Pt. (f) Typical data of the resistance change during the hydrogenation and NRA measurements for $SmNiO_3$. Hydrogen gas was introduced in the vacuum chamber at the times indicated by blue arrows, where the resistance changes due to the temperature control and hydrogenation of the sample.

separation distance of 5 μm and a thickness of about 20 nm was fabricated on top of the films by a photolithography technique [21]. To measure the sample resistance, Pt films with a width of 1 mm were deposited at the edges of the sample. After transferring the pristine samples into the vacuum chamber (base pressure 2×10^{-5} Pa) for a nuclear reaction analysis, the samples were *in situ* hydrogenated under an H_2 gas at a sample temperature of 480 K. At this temperature, oxygen vacancy formation may be neglected according to previous studies [15,22]. The sample resistance was *in situ* monitored during the hydrogenation of the sample and a subsequent NRA measurement as shown in Fig. 1(f) as measured for $SmNiO_3$, where the resistance increases and decreases as the hydrogenation proceeds; for details and the data for other samples, see the Supplemental Material [23]. The measurements of NRA via $^1H(^{15}N, \alpha\gamma)^{12}C$ were conducted at the 2C beamline of Micro Analysis Laboratory (MALT) in the University of Tokyo with a $^{15}N^{2+}$ ion current of 20–50 nA and a beam size of about 3×3 mm^2 on the sample in normal incidence [16,17]. The NRA yield is displayed as γ-ray counts due to the reaction normalized to the beam dose. The stopping power for the samples ($R NiO_3H_x$) was calculated from the stopping cross section of each element [16]. Since the ion stopping due to hydrogen is small, the depth scale in the NRA yield curve is shown by assuming $x = 0$. Because the NRA yield depends on the stopping power and the composition including the hydrogen concentration, the hydrogen concentration was evaluated by solving the self-consistent equation [23].

III. RESULTS AND DISCUSSION

As shown in Fig. 2(a), thermal MIT was confirmed for $SmNiO_3$ and $NdNiO_3$ at ∼360 and ∼150 K, respectively, and a metallic feature was observed for $LaNiO_3$, which are consistent with a previous study [1]. Note the raw resistance data are shown in this paper instead of the resistivity, because the hydrogenation of some samples was inhomogeneous either in the in-plane or depth direction as shown below. Figures 3(a)–3(c) show the NRA yield curves corresponding to the H depth distribution acquired after various hydrogenation treatments. Before the hydrogenation, the profile reveals a peak at a depth of 0 nm and a small intensity corresponding to $x \lesssim 0.1$ in a depth region of 30–90 nm. The peak at 0 nm corresponds to a surface-adsorbed hydrogen species including possible contaminations. As the hydrogenation proceeds, the hydrogen concentration in the film increases up to $x \sim 1$ with the surface peak constant. The profiles exhibit distinct dips at 10–20 nm, which are mainly due to the mesh-patterned Pt layer deposited on the surface for H_2 dissociation; compared to the bare part of the sample, the $^{15}N^{2+}$ ion beam incident to the Pt-covered part suffers from an additional energy loss in the Pt layer, which does not absorb hydrogen. The H concentration gradually decreases at about 80 nm and little hydrogen is observed at a depth of deeper than 120 nm. This indicates that H does not diffuse into the substrate. Taking account of the energy loss in the Pt layer, the overall NRA profile was decomposed into two components of the regions with and without the Pt layer, which are shifted in energy by the amount of the energy loss due to the Pt layer [23]. Assuming the H concentration in the sample is uniform, the NRA data are described by Eq. (1) in the Supplemental Material [23]: Typical results of analysis for $SmNiO_3$ and $NdNiO_3$ are shown in Fig. 3(d). Note that the areal ratio of the Pt-covered region obtained from the analysis for $NdNiO_3$ is larger than the nominal area of the Pt-covered region of the sample. This suggests the H diffusion is faster at the Pt-substrate interface than the bare region. While the curves for $SmNiO_3$ and $NdNiO_3$ exhibit rather uniform depth distributions, those measured for $LaNiO_3$ are different; the profile initially reveals an enhanced intensity at a depth of 90 nm and a slight hump at 30 nm with an almost uniform intensity at 50–70 nm. With increasing hydrogenation time,

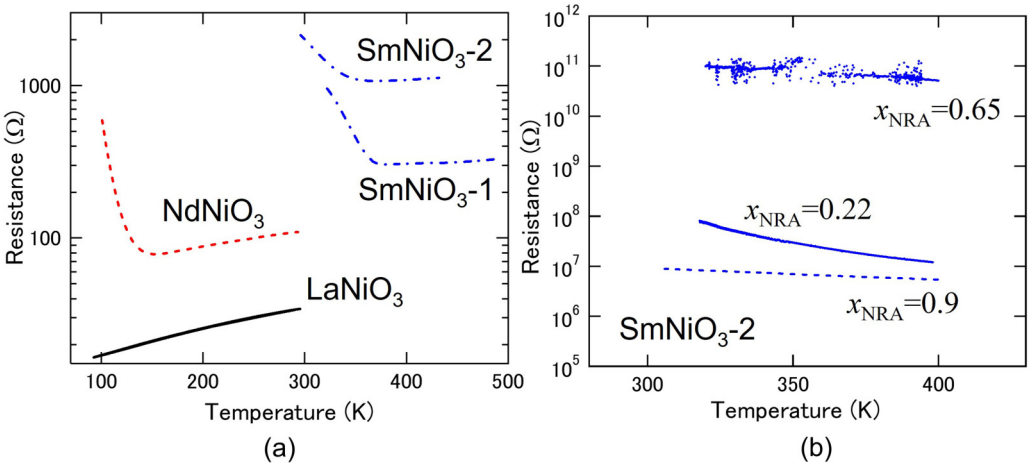

FIG. 2. Resistance as a function of temperature for the RNiO$_3$ (R = Sm, Nd, and La) samples (a) before and (b) after hydrogenation. In (a), SmNiO$_3$-1 is the result of the pristine sample, and SmNiO$_3$-2 is the result after a cycle of hydrogenation and dehydrogenation. Note that the resistance was almost recovered to the initial condition after the cycle, although the resistance was slightly higher and the MIT temperature was slightly lower. In (b), the temperature dependence of the resistance of SmNiO$_3$-2 at three hydrogenation stages is shown. Due to the high resistance, the measurement was not stable at $x_{\mathrm{NRA}} = 0.65$.

the intensity increases and eventually the entire profile appears to be almost uniform. This result indicates that the H concentration is not uniform in the depth direction for LaNiO$_3$ depending on the hydrogenation stage in contrast to the rather uniform distributions for SmNiO$_3$ and NdNiO$_3$. Therefore, the analysis result for LaNiO$_3$ is not shown in Fig. 3(d).

Figure 4 shows the resistance of the samples as a function of the hydrogen concentration (x_{NRA}), where x_{NRA} was obtained as the average H concentration in the film from the analysis of Fig. 3 taking account of the Pt layer. Note the small marks for x_{NRA} of LaNiO$_3$ denotes the large concentration at the near-interface region and the small concentration at the middle of the film reflecting the nonuniform depth distribution of H in the sample. As for SmNiO$_3$, the resistance increases to $\sim 10^9$ Ω at $x_{\mathrm{NRA}} \sim 0.2$ and reaches a maximum at $x_{\mathrm{NRA}} \sim 0.5$, followed by a decrease at $x_{\mathrm{NRA}} \sim 1$. The resistance as a function of temperature at three hydrogenation stages is shown in Fig. 2(b). It should be noted that the resistance behavior at $x_{\mathrm{NRA}} \sim 1$ is different in the two measurements. The cycle of hydrogenation and dehydrogenation might have caused some structural change, which is also recognized by the difference in the MIT temperature in Fig. 2(a). Whereas the data for NdNiO$_3$ and LaNiO$_3$ also show a resistance increase at $x_{\mathrm{NRA}} \sim 0.2$ followed by a saturating behavior at $x_{\mathrm{NRA}} \sim 0.4$, the amount of the resistance increase is much smaller than that of SmNiO$_3$ and the decreasing behavior at $x_{\mathrm{NRA}} \sim 1$ is not observed. Note LaNiO$_3$ also shows an H-induced MIT, which is in contrast to the result of a previous study [9]. This is probably due to the difference in the hydrogenation temperature and pressure. Since the hydrogenation was performed at 480 K in the present study, which is higher than that in a previous study, the hydrogenation was fast and a highly hydrogenated state was realized in this study.

The present experimental results clearly show that an H-induced MIT starts to occur at $x_{\mathrm{NRA}} \sim 0.2$ for the three RNiO$_3$ (R = Sm, Nd, and La) films. The difference in the amount of the resistance increase at $x_{\mathrm{NRA}} \sim 0.2$ between the three samples in Fig. 4 originates from the homogeneity of the hydrogenation of the samples. Because H atoms are incorporated into the films via dissociation at the Pt islands deposited on the samples, the samples might not be uniformly hydrogenated [21]. The images shown in Fig. 4 are the optical transmission microscope images taken at the hydrogenation stages indicated by arrows in the figure. The black squares in the images correspond to the mesh-patterned Pt layer, and the bright region corresponds to the bare RNiO$_3$ film. In the case of SmNiO$_3$, the bare region becomes uniformly brighter, suggesting that the entire sample was hydrogenated, although part of the sample looks even brighter at a high resistance; see a large-scale image in the Supplemental Material [23]. On the other hand, middle part of the bare region remains dark clearly for NdNiO$_3$ and slightly for LaNiO$_3$. These results indicate that middle part is not hydrogenated for R = Nd and La, because hydrogen diffusion is not sufficient for the two samples [21,24]. As for the R = La sample, furthermore, the depth distribution is not uniform; the H concentration is enhanced in the near-interface regions between Pt and LaNiO$_3$ and between LaNiO$_3$ and the substrate. From these results, it is concluded the effects of inhomogeneity are significant for R = Nd and La, whereas the entire sample of R = Sm is rather uniformly hydrogenated by exposure to H$_2$ gas. Hence, it is considered that the curve for the R = Sm sample in Fig. 4 reflects the actual relation between the resistance and hydrogen concentration.

We first discuss the H-induced MIT for R = Sm and the data for R = Nd and La are discussed later. Two possible interpretations for the steep increase at $x_{\mathrm{NRA}} \sim 0.2$ with a saturating trend at $x_{\mathrm{NRA}} \sim 0.5$ are conceived: One is that SmNiO$_3$ is in a highly insulating state in the range of $\sim 0.2 \leqslant x \leqslant 0.5$, and the other is that there is an insulating state at $x = 0.5$ and that a microscopic phase separation into H-rich and H-poor regions occurs. If the effective H-H interaction is attractive, H atoms tend to accumulate forming H-rich domains whereas other regions become H poor. In this case, the

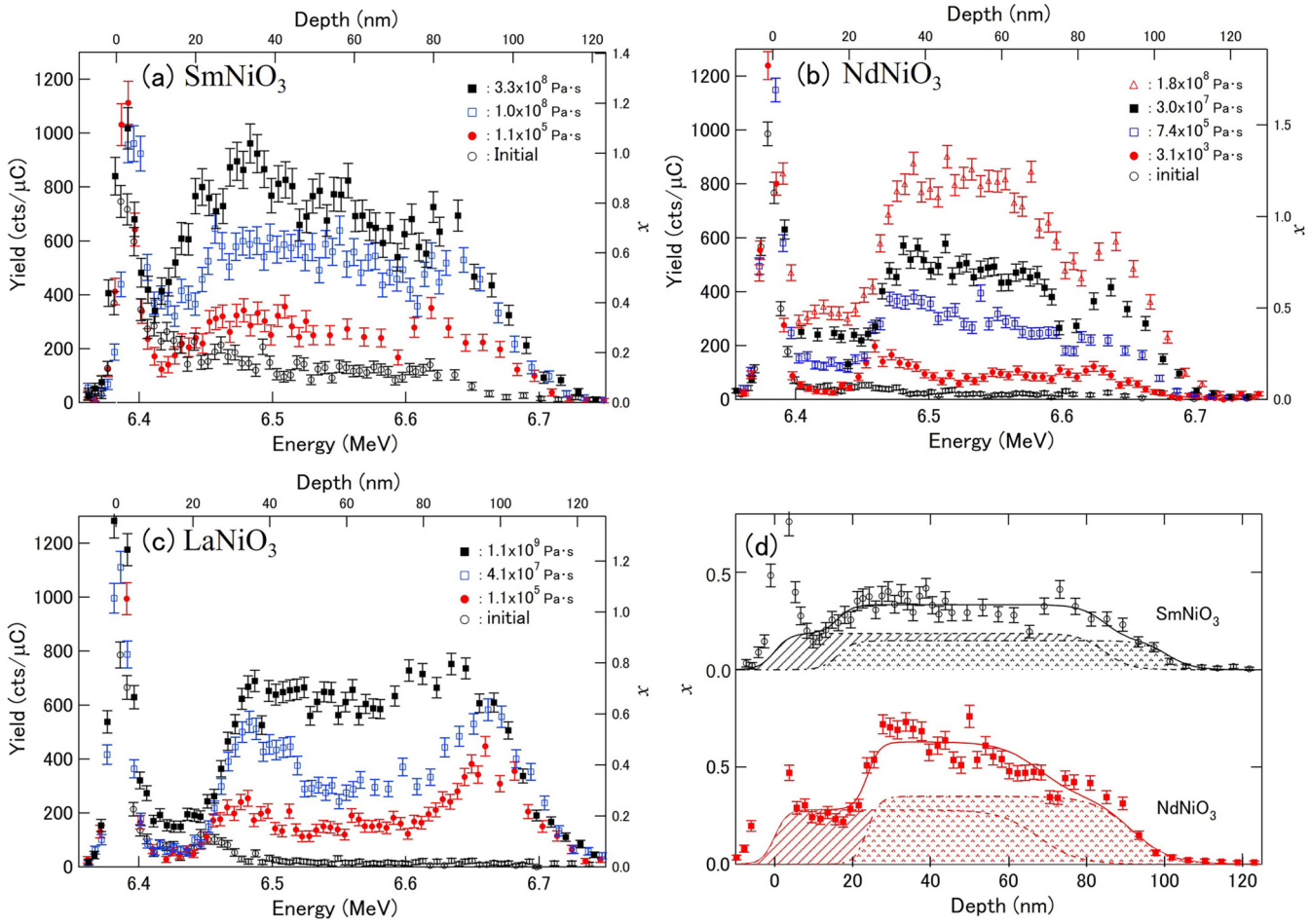

FIG. 3. NRA yield curves measured for (a) $SmNiO_3$, (b) $NdNiO_3/LaAlO_3(001)$, and (c) $LaNiO_3$ after various exposures to H_2 at a sample temperature of 480 K. Hydrogen concentration (x) obtained after calibration of the detection efficiency is shown at the right ordinate. (d) Decomposition analysis into two components originating from bare and Pt-covered regions. Shaded curves are the decomposed constituents of $SmNiO_3$ (1.1×10^5 Pa s) and $NdNiO_3/LaAlO_3(001)$ (7.4×10^5 Pa s), which are shifted in energy corresponding to the energy loss in the Pt layer.

resistance behavior represents the percolation of the H-poor low-resistance domains. The percolation threshold, where the resistance becomes high, is 30%–70% of the volume depending on the dimensionality [25]. Since the resistance increases at $x_{NRA} \sim 0.2$, the hydrogen concentration for the H-rich insulating state of $x = 0.5$ is consistent with the percolation mechanism. Although the former possibility cannot be ruled out at the present stage, we can unambiguously conclude that an insulating phase exists at $x \sim 0.5$ in both cases, which we call phase A. With increasing x, furthermore, the resistance decreases at $x_{NRA} \sim 1.0$. Considering the resistance is as high as 10^6 Ω at $x_{NRA} \sim 1.0$ and the temperature dependence of the resistance exhibits a nonmetallic feature, the results suggest there is another insulating state at $x = 1.0$ different from phase A, which we call phase B. It should be noted that the insulating state of $x = 0.5$ is not formed by a mixture of the phase-separated states of $x = 0$ and $x = 1.0$, because the resistances of the latter two are much lower than that at $x = 0.5$. In a previous study [10], it seems that the hydrogenated region around Pt catalysts consists of regions with different contrasts as observed in an optical image. This might correspond to the two phases confirmed in the present study.

We discuss the electronic mechanism for the H-induced MIT of $SmNiO_3$. In $RNiO_3$, nickel atoms are nominally in the Ni^{3+} state with a formal electronic configuration of $3d^7$ ($t_{2g}^6 e_g^1$). Doping of hydrogen brings about the reduction of Ni ions as confirmed by XPS [10,26]. Since hydrogen has one electron, fully reducing Ni^{3+} to Ni^{2+} needs doping of H with $x = 1$. However, the present results show that MIT is induced at $x = 0.5$ as well as $x = 1$. It is known that the thermally induced MIT is accompanied by a structural distortion of NiO_6 octahedra into sets of compressed and expanded octahedra [27], which is schematically shown in Fig. 1(b). In view of this scenario, as one of the possible mechanisms, we propose that a hydrogen doping at $x = 0.5$ stabilizes the distorted structure as schematically shown in Fig. 1(d), where two inequivalent Ni sites are present and three electrons are present in these two units. A previous theoretical study has shown that integer filling of degenerate states results in a Mott insulating state, which suggests both Ni sites could be insulating, leading to an entire insulator [28]. A recent theoretical study, furthermore, has shown that $SmNiO_3H_{0.5}$ can be an insulator with a periodicity of 2×1 [29], which is qualitatively consistent with the present result.

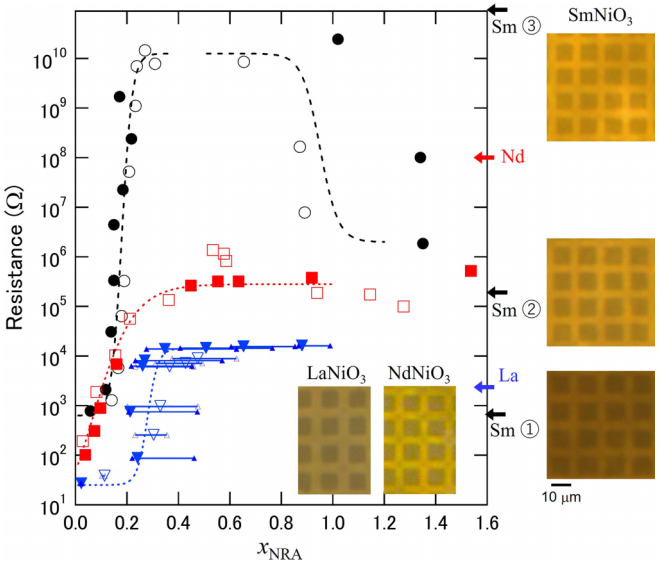

FIG. 4. Resistance at 330 K for $SmNiO_3$ (black circle), $NdNiO_3$ (red square), and $LaNiO_3$ (blue triangle) as a function of the hydrogen concentration (x_{NRA}). x_{NRA} was estimated from the intensity at the plateau region as obtained by the analysis of NRA yield curves. Two plots for $SmNiO_3$ are the first (black solid circle) and second (black open circle) measurements of an identical sample: The second set of measurements was conducted after dehydrogenation of the hydrogenated sample by heating at 480 K in air. Two plots for $NdNiO_3$ are the measurements for $NdNiO_3/SrTiO_3(001)$ (red solid square) and $NdNiO_3/LaAlO_3(001)$ (red open square). Two plots for $LaNiO_3$ are the measurements for two samples. Dashed curves are guides for the eyes. For $LaNiO_3$, large and small concentrations at the interface and middle of the film are shown by small triangles. Also shown are the optical transmission microscope images for the three samples taken at the hydrogenation stages indicated by arrows as observed by the sample resistance in separate experiments. Note that the resistance increase for $NdNiO_3$ was larger than that measured for NRA.

At $x = 1.0$, on the other hand, the $RNiO_3H_1$ phase corresponds to the $3d^8$ ($t_{2g}^6 e_g^2$) Mott insulating phase as shown in Fig. 1(c), which was theoretically confirmed with first-principles calculations [22,30,31]. Interestingly, this phase B has a lower resistance compared to phase A at $x = 0.5$. The incorporation of hydrogen might induce a large structural distortion at phase A, which possibly modifies the electronic structure shown in Fig. 1(d). These results definitely indicate the two Mott states can be switched by H doping. Furthermore, we point out H doping at x of larger than 1 can be realized for $SmNiO_3$ and $NdNiO_3$, which leads to an overdoped phase [15]. Although the resistance remains unchanged at $x > 1.0$, this points to a possibility of heavy hydrogen doping, which could open up a different paradigm in the strongly correlated system.

Based on the above model of dual Mott states, we discuss the resistance behavior of $NdNiO_3$ and $LaNiO_3$ assuming that similar two insulating phases of phase A and phase B with high and low resistances are present at $x = 0.5$ and $x = 1.0$, respectively. As observed in the optical image, only the region near Pt islands is hydrogenated, and it is expected that both phase A and phase B coexist in this region. Hence, the experimentally measured resistance in Fig. 4 reflects the combined resistance of the hydrogenated phases and nonhydrogenated phase in series. As the hydrogenation proceeds, the portion of phase A might remain small while the hydrogenated region expands. In this case, the combined resistance does not become as high as 10^{10} Ω of phase A throughout the hydrogenation process. At a fully hydrogenated state, the resistance becomes that of phase B, which seems to be consistent with the result of Fig. 4. As for $LaNiO_3$, inhomogeneity in the depth direction needs to be considered: The experimentally measured resistance represents the combined resistance of the near-interface and middle regions of the film in parallel. Considering the H depth distribution at an initial hydrogenation stage, the near-interface region is hydrogenated as phase A, while the middle region is only slightly hydrogenated. When the middle region is hydrogenated as phase A, on the other hand, the near-interface region becomes phase B with a lower resistance. Therefore, the combined resistance does not become as high as 10^{10} Ω as $SmNiO_3$. It should be noted that a highly insulating state corresponding to phase A can also be realized for $NdNiO_3$ and $LaNiO_3$ in a different hydrogenation approach [32].

In conclusion, by developing an apparatus to *in situ* measure the resistance and hydrogen concentration of the sample with NRA, we have clarified the detailed relation between the resistance and hydrogen concentration of $RNiO_3$ (R = Sm, Nd, and La). The three samples revealed a resistance increase at $x_{NRA} \sim 0.2$. The H depth distribution and optical images show that hydrogenation is inhomogeneous for $NdNiO_3$ and $LaNiO_3$. In contrast to these two samples, $SmNiO_3$ was uniformly hydrogenated. From the relation of the resistance and hydrogen concentration of $SmNiO_3$, it is found that a highly insulating phase is formed at $x = 0.5$ and another insulating phase is formed at $x = 1.0$, both of which are attributed to Mott insulating states. This indicates the dual Mott states can be reversibly switched by the hydrogen doping level. A detailed structural and electronic analysis of the hydrogenated $RNiO_3$ taking account of negative charge transfer between Ni and O [4,5] is required for further understanding the Mott phases.

ACKNOWLEDGMENTS

This work was performed under the Cooperative Research Program of "Network Joint Research Center for Materials and Devices," and supported by a JSPS KAKENHI Grant-in-Aid for Scientific Research on Innovative Areas "Hydrogenomics" (Grant No. JP18H05518) and Scientific Research (Grants No. JP21H04650 and No. JP22K14600). The authors thank H. Matsuzaki, H. Tokuyama, and T. Yamagata for their assistance in the accelerator operation.

[1] J. B. Torrance, P. Lacorre, A. I. Nazzal, E. J. Ansaldo, and C. Niedermayer, Phys. Rev. B **45**, 8209 (1992).

[2] M. L. Medarde, J. Phys.: Condens. Matter **9**, 1679 (1997).

[3] G. Catalan, Phase Transitions **81**, 729 (2008).
[4] T. Mizokawa, D. I. Khomskii, and G. A. Sawatzky, Phys. Rev. B **61**, 11263 (2000).
[5] V. Bisogni, S. Catalano, R. J. Green, M. Gibert, R. Scherwitzl, Y. Huang, V. N. Strocov, P. Zubko, S. Balandeh, J.-M. Triscone, G. Sawatzky, and T. Schmitt, Nat. Commun. **7**, 13017 (2016).
[6] H. Park, A. J. Millis, and C. A. Marianetti, Phys. Rev. Lett. **109**, 156402 (2012).
[7] S. Johnston, A. Mukherjee, I. Elfimov, M. Berciu, and G. A. Sawatzky, Phys. Rev. Lett. **112**, 106404 (2014).
[8] A. Subedi, O. E. Peil, and A. Georges, Phys. Rev. B **91**, 075128 (2015).
[9] J. Chen, Y. Zhou, S. Middey, J. Jiang, N. Chen, L. Chen, X. Shi, M. Dobeli, J. Shi, J. Chakhalian, and S. Ramanathan, Appl. Phys. Lett. **107**, 031905 (2015).
[10] J. Shi, Y. Zhou, and S. Ramanathan, Nat. Commun. **5**, 4860 (2014).
[11] Z. Zhang, D. Schwanz, B. Narayanan, M. Kotiuga, J. A. Dura, M. Cherukara, H. Zhou, J. W. Freeland, J. Li, R. Sutarto, F. He, C. Wu, J. Zhu, Y. Sun, K. Ramadoss, S. S. Nonnenmann, N. Yu, R. Comin, K. M. Rabe, S. K. R. S. Sankaranarayanan *et al.*, Nature (London) **553**, 68 (2018).
[12] Y. Zhou, X. Guan, H. Zhou, K. Ramadoss, S. Adam, H. Liu, S. Lee, J. Shi, M. Tsuchiya, D. D. Fong, and S. Ramanathan, Nature (London) **534**, 231 (2016).
[13] H.-T. Zhang, T. J. Park, A. N. M. N. Islam, D. S. J. Tran, S. Manna, Q. Wang, S. Mondal, H. Yu, S. Banik, S. Cheng, H. Zhou, S. Gamage, S. Mahapatra, Y. Zhu, Y. Abate, N. Jiang, S. K. R. S. Sankaranarayanan, A. Sengupta, C. Teuscher, and S. Ramanathan, Science **375**, 533 (2022).
[14] J. Chen, W. Mao, L. Gao, F. Yan, T. Yajima, N. Chen, Z. Chen, H. Dong, B. Ge, P. Zhang, X. Cao, M. Wilde, Y. Jiang, T. Terai, and J. Shi, Adv. Mater. **32**, 1905060 (2020).
[15] J. Chen, W. Mao, B. Ge, J. Wang, X. Ke, V. Wang, Y. Wang, M. Dobeli, W. Geng, H. Matsuzaki, J. Shi, and Y. Jiang, Nat. Commun. **10**, 694 (2019).
[16] M. Wilde and K. Fukutani, Surf. Sci. Rep. **69**, 196 (2014).
[17] K. Fukutani, Curr. Opin. Solid State Mater. Sci. **6**, 153 (2002).
[18] H. Yoon, M. Choi, T.-W. Lim, H. Kwon, K. Ihm, J. K. Kim, S.-Y. Choi, and J. Son, Nat. Mater. **15**, 1113 (2016).
[19] N. Lu, P. Zhang, Q. Zhang, R. Qiao, Q. He, H.-B. Li, Y. Wang, J. Guo, D. Zhang, Z. Duan, Z. Li, M. Wang, S. Yang, M. Yan, E. Arenholz, S. Zhou, W. Yang, L. Gu, C.-W. Nan, J. Wu *et al.*, Nature (London) **546**, 124 (2017).
[20] Y. Yamashita, G. Lim, T. Maruyama, A. Chikamatsu, T. Hasegawa, H. Ogino, T. Ozawa, M. Wilde, K. Fukutani, T. Terashima, M. Ochi, K. Kuroki, H. Kitagawa, and M. Maesato, Phys. Rev. B **104**, L041111 (2021).
[21] U. Sidik, A. N. Hattori, K. Hattori, M. Alaydrus, I. Hamada, L. N. Pamasi, and H. Tanaka, ACS Appl. Electron. Mater. **4**, 4849 (2022).
[22] M. Kotiuga, Z. Zhang, J. Li, F. Rodolakis, H. Zhou, R. Sutarto, F. He, Q. Wang, Y. Sun, Y. Wang, N. A. Aghamiri, S. B. Hancock, L. P. Rokhinson, D. P. Landau, Y. Abate, J. W. Freeland, R. Comin, S. Ramanathan, and K. M. Rabe, Proc. Natl. Acad. Sci. USA **116**, 21992 (2019).
[23] See Supplemental Material at http://link.aps.org/supplemental/10.1103/PhysRevMaterials.7.085003 for the experimental procedure showing the resistance evolution during the measurement; the analysis of the nuclear reaction profiles; the analysis formula for the hydrogen concentration in samples; and the large-scale optical image of $SmNiO_3$, which includes Refs. [16,17].
[24] U. Sidik, A. N. Hattori, H.-B. Li, S. Nonaka, A. I. Osaka, and H. Tanaka, Appl. Phys. Express **16**, 014001 (2023).
[25] M. B. Isichenko, Rev. Mod. Phys. **64**, 961 (1992).
[26] T. Yamanaka, A. N. Hattori, L. N. Pamasi, S. Takemoto, K. Hattori, H. Daimon, K. Sato, and H. Tanaka, ACS Appl. Electron. Mater. **1**, 2678 (2019).
[27] J. A. Alonso, M. J. Martínez-Lope, M. T. Casais, J. L. García-Muñoz, and M. T. Fernández-Díaz, Phys. Rev. B **61**, 1756 (2000).
[28] M. J. Rozenberg, Phys. Rev. B **55**, R4855(R) (1997).
[29] K. Yamauchi and I. Hamada, Phys. Rev. B **108**, 045108 (2023).
[30] L. Iglesias, M. Bibes, and J. Varignon, Phys. Rev. B **104**, 035123 (2021).
[31] P. Yoo and P. Liao, Phys. Chem. Chem. Phys. **22**, 6888 (2020).
[32] I. Matsuzawa, T. Ozawa, Y. Nishiya, U. Sidik, A. Hattori, H. Tanaka, and K. Fukutani (unpublished).